ResearchGate

See discussions, stats, and author profiles for this publication at: https://www.researchgate.net/publication/227000833

Parameterization of Heat and Moisture Transfer in the Soil–Vegetation System for Use in Atmospheric General Circulation Models: 2. Numerical Experiments in Climate Modeling

Article in Izvestiya Atmospheric and Oceanic Physics · September 1998

CITATIONS
15

2 authors:

Evgeny Volodin
147 PUBLICATIONS · **3,402** CITATIONS
SEE PROFILE

READS
139

Vasily N. Lykosov
Russian Academy of Sciences
197 PUBLICATIONS · **2,149** CITATIONS
SEE PROFILE

Some of the authors of this publication are also working on these related projects:

Project Dynamic modelling of climate changes in the Black Sea area in XXI century View project

All content following this page was uploaded by Vasily N. Lykosov on 05 January 2015.
The user has requested enhancement of the downloaded file.

Izvestiya, Atmospheric and Oceanic Physics, Vol. 34, No. 5, 1998, pp. 559–569. Translated from Izvestiya AN. Fizika Atmosfery i Okeana, Vol. 34, No. 5, 1998, pp. 622–633.
Original Russian Text Copyright © 1998 by Volodin, Lykosov.
English Translation Copyright © 1998 by МАИК Наука/Interperiodica Publishing (Russia).

Parametrization of Heat and Moisture Transfer in the Soil–Vegetation System for Use in Atmospheric General Circulation Models: 2. Numerical Experiments in Climate Modeling

E. M. Volodin and V. N. Lykosov

Institute of Numerical Mathematics, Russian Academy of Sciences, Leninskii pr. 32a, Moscow, 117334 Russia

Received October 25, 1996; in final form, January 21, 1997

Abstract—The parametrization scheme of heat and moisture transfer in the soil–vegetation system suggested in [1] is used within the atmospheric general circulation model being developed at the Institute of Numerical Mathematics, Russian Academy of Sciences. Simulated seasonal variations in the surface air temperature and the land hydrologic cycle are compared with those obtained with a simplified treatment of soil processes. The sensitivity of model circulation to the degree of detail in the specification of soil and vegetation types is analyzed. Relevant data on these parameters used in the general circulation model are given. On the whole, the parametrization proposed is found promising for use in climate studies.

INTRODUCTION

In Part 1 of this study [1], we proposed a locally one-dimensional model of heat and moisture transfer in soil, whose surface can be bare, vegetated, or snow-covered, depending on geographic conditions and the season. A new element in this parametrization as compared to those used earlier in global models is a rather detailed description of heat and moisture diffusion in the soil and, especially, the introduction of all three states of water and the phase transitions between them. The model was run in a stand-alone mode [1]. As input model parameters, actual observations of time-varying air temperature and snow depth were taken in simulations of the soil freezing process and atmospheric characteristics (wind velocity, temperature, humidity, and precipitation) were used in more complete validation of the model. A comparison showed that the model results agree rather well with available observational data, which suggests a possibility of using this parametrization within atmospheric general circulation models (GCMs).

This parametrization scheme was incorporated into the atmospheric GCM being developed at the Institute of Numerical Mathematics, Russian Academy of Sciences [2]. The version used had a 5° longitude by 4° latitude spatial resolution and 13 levels in the vertical. The model included a complete set of physical parametrizations and made allowance for the annual and diurnal cycles of the sun's declination. The sea surface temperature and the sea ice were specified by the geographic distributions observed for September 1985–August 1988. This model was modified by introducing the detailed description of soil heat and moisture transfer and was then run in two experiments. The first (called experiment I) made allowance for geographic diversity of soils and vegetation, and the second (called experiment II) did not. In both experiments, the model was integrated for 4 years. The first year was not analyzed, because this period is needed to achieve the model climate from the initial data specified by atmospheric and soil distributions, which are inconsistent in general. The control experiment with a preliminary version of soil–vegetation parametrization [2] was conducted in a similar way. In that version, the soil was represented by a single layer with a water capacity of 0.35 m, no allowance was made for soil freezing, the stomatal resistance depended only on the soil water content and was equal to 25 s/m at its sufficient value, and the heat flux from the soil to the ground surface was proportional to the difference between the surface soil temperature and the unvarying deep soil temperature at a depth of 2 m.

In this paper, we describe some results of these numerical experiments and their comparative analysis. In Section 1, we discuss simulated seasonal temperature variations. The land hydrologic cycle is examined in Section 2. In Section 3, we analyze the model sensitivity to the degree of detail in the specification of soil and vegetation types. Finally, Appendixes 1 and 2 present relevant data on the soil and vegetation types used in the GCM.

1. SIMULATED SEASONAL TEMPERATURE VARIATIONS

Primary attention in our analysis is given to the comparison of observed surface air temperatures with those calculated in experiment I and in the control experiment [3, 4]. Figure 1 shows the zonally averaged

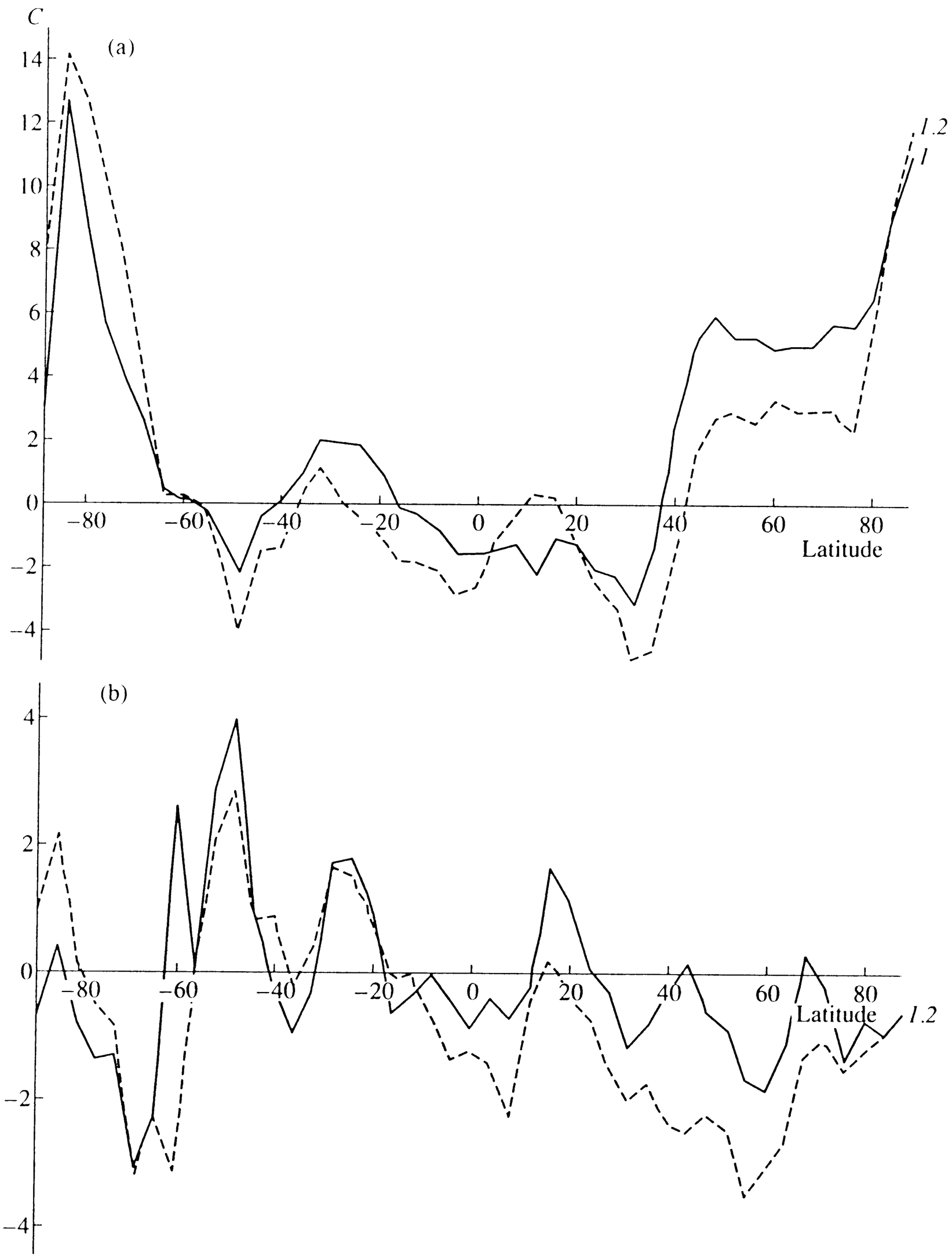

Fig. 1. Zonally averaged difference between the simulated and observed surface air temperature over continents and sea and land ices for (a) January and (b) July. Solid lines correspond to experiment I (model with a soil–vegetation parametrization), and dashed lines indicate the control experiment.

differences between the simulated and observed surface air temperatures (at a height of 2 m) over land and sea–land ices in the two experiments for (a) January and (b) July. The global features of the simulated temperature fields can be seen clearly in these figures. For January, the error of the reproduced temperature in experiment I is as large as 8–12 degrees in the Arctic region and Antarctica, is about four degrees in the midlatitudes of both hemispheres, and is within two degrees in the tropics. For July, the simulated 2-m temperatures are, on the whole, very close to the observed fields, which suggests correct redistribution of the surface radiative balance between evaporation and sensible heat flux. In the control experiment, there is a small negative bias in the July temperature in the Northern Hemisphere.

Figure 2 shows contour maps of monthly mean differences between the simulated (with the improved

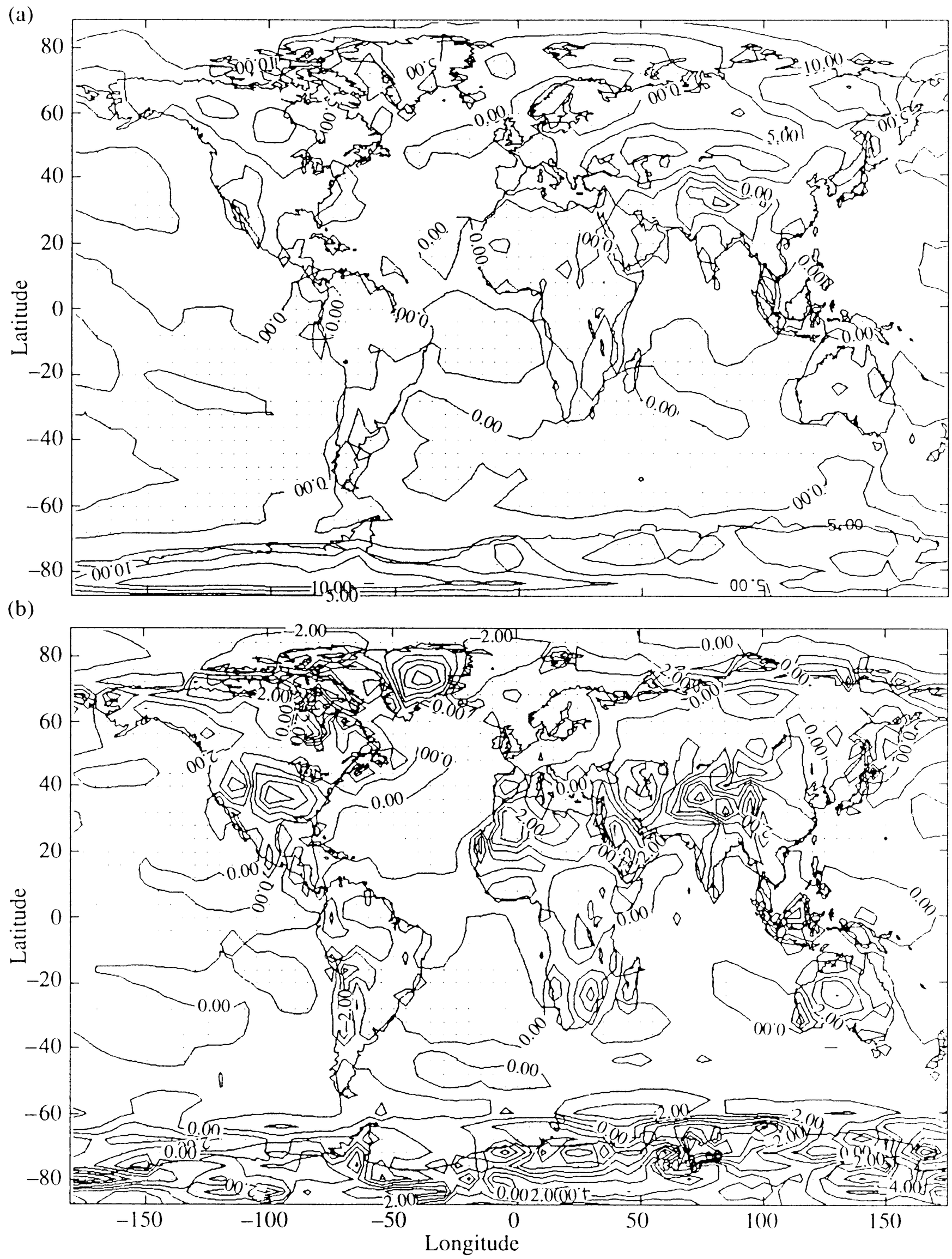

Fig. 2. Difference between the simulated (experiment I) and observed surface air temperature for (a) January and (b) July. The contour intervals are 5 and 2 degrees for January and July, respectively.

soil–vegetation parametrization) and observed 2-m air temperatures for (a) January and (b) July. First, let us discuss the results obtained for the winter season. It is evident from Fig. 2a that there is a positive bias up to 5–15 degrees in the simulated temperature over the snow-covered land and polar sea and land ices for the winter season. This bias in experiment I (detailed formulation of soil processes) was found to be 2–4 degrees larger than that in the control experiment.

A plausible cause of this bias, found in both model versions, may be an insufficiently complete description of the heat transfer between the ice surface and the

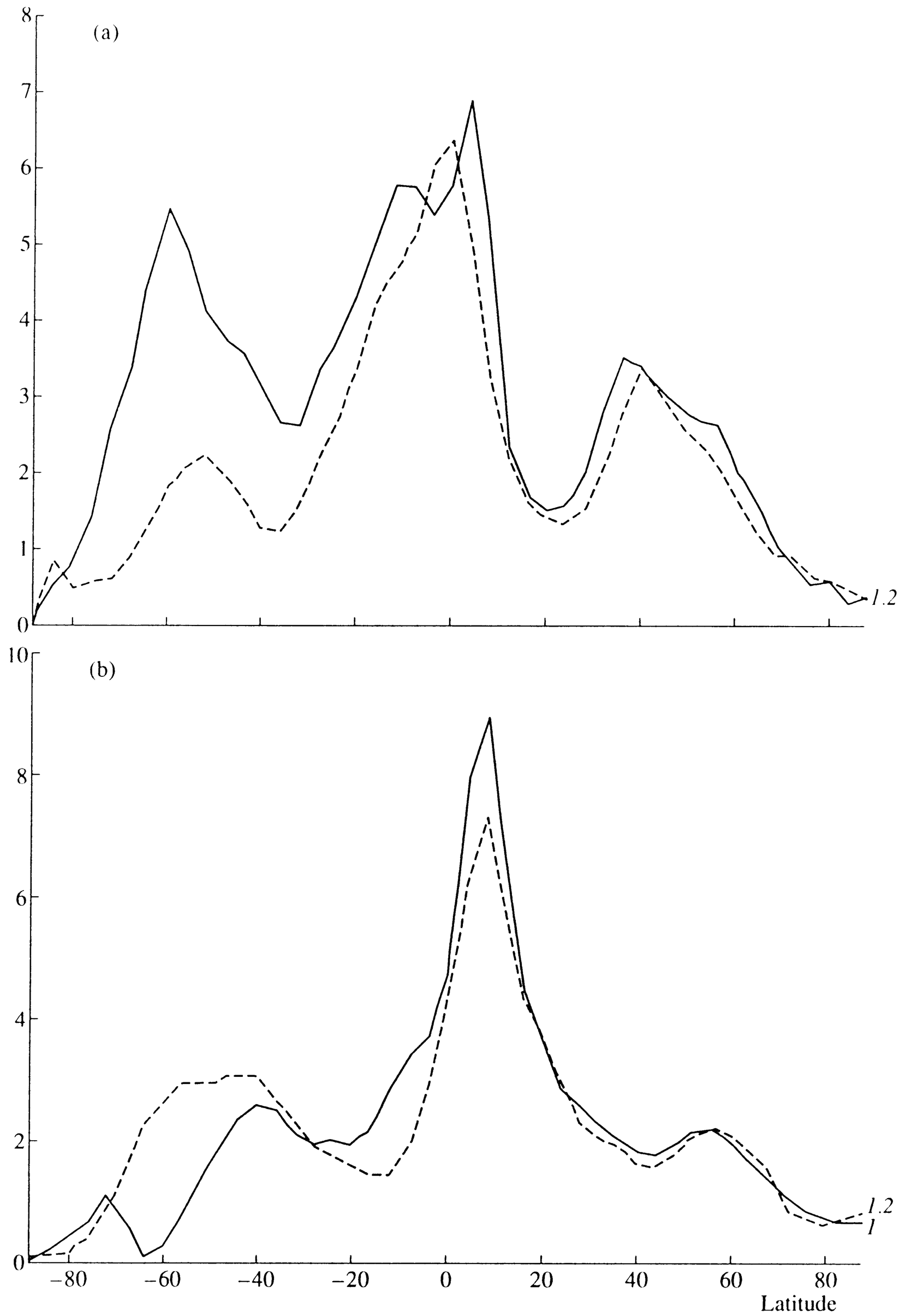

Fig. 3. Zonally averaged observed (solid) and simulated (dashed) precipitation (mm/day) for (a) January and (b) July.

underlying seawater. Specifically, it is customary to specify an artificial lower limit of the ice surface temperature in models. The second cause is possibly that the model albedo of a snow-covered surface cannot exceed 0.6. This constraint seems valid for geometrically inhomogeneous snow-covered surfaces, which include, for example, snow-free trees or rocks. However, under homogeneous conditions, for example, over

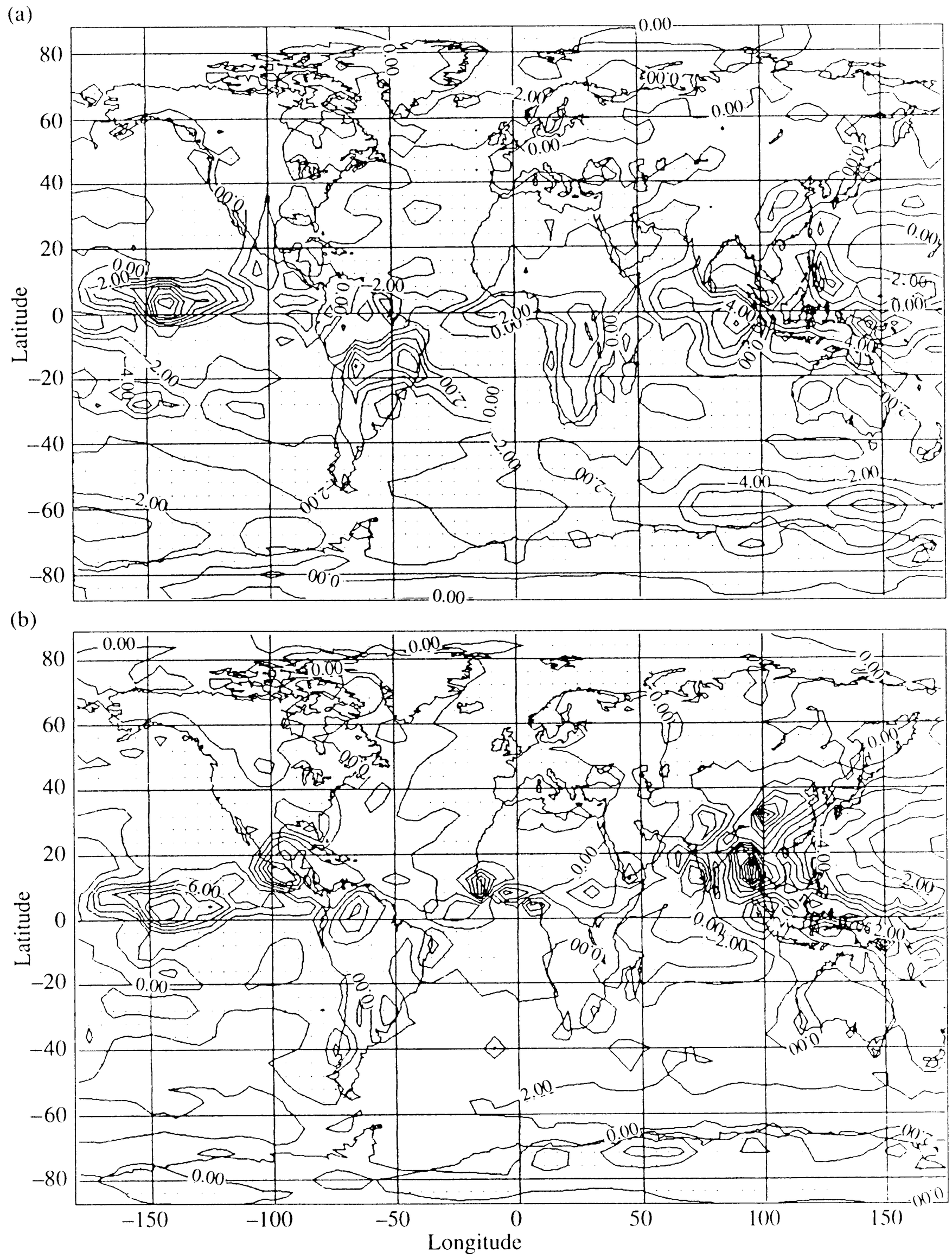

Fig. 4. Difference between simulated (experiment I) and observed precipitation (mm/day) for (a) January and (b) July. The contour interval is 2 mm/day.

steppes, tundra, Greenland, or Antarctica, the albedo of snow at low temperatures may be much greater than 0.6. As can be seen in Fig. 2a, the bias in the simulated wintertime surface air temperature is maximum for these regions. An increase in this bias in experiment I can be explained by increased heat flux from the surface as compared to that in the control experiment. This is associated with a more detailed calculation of heat transfer in a multi-layer soil and with allowance made for water freezing in the soil, which results in relatively

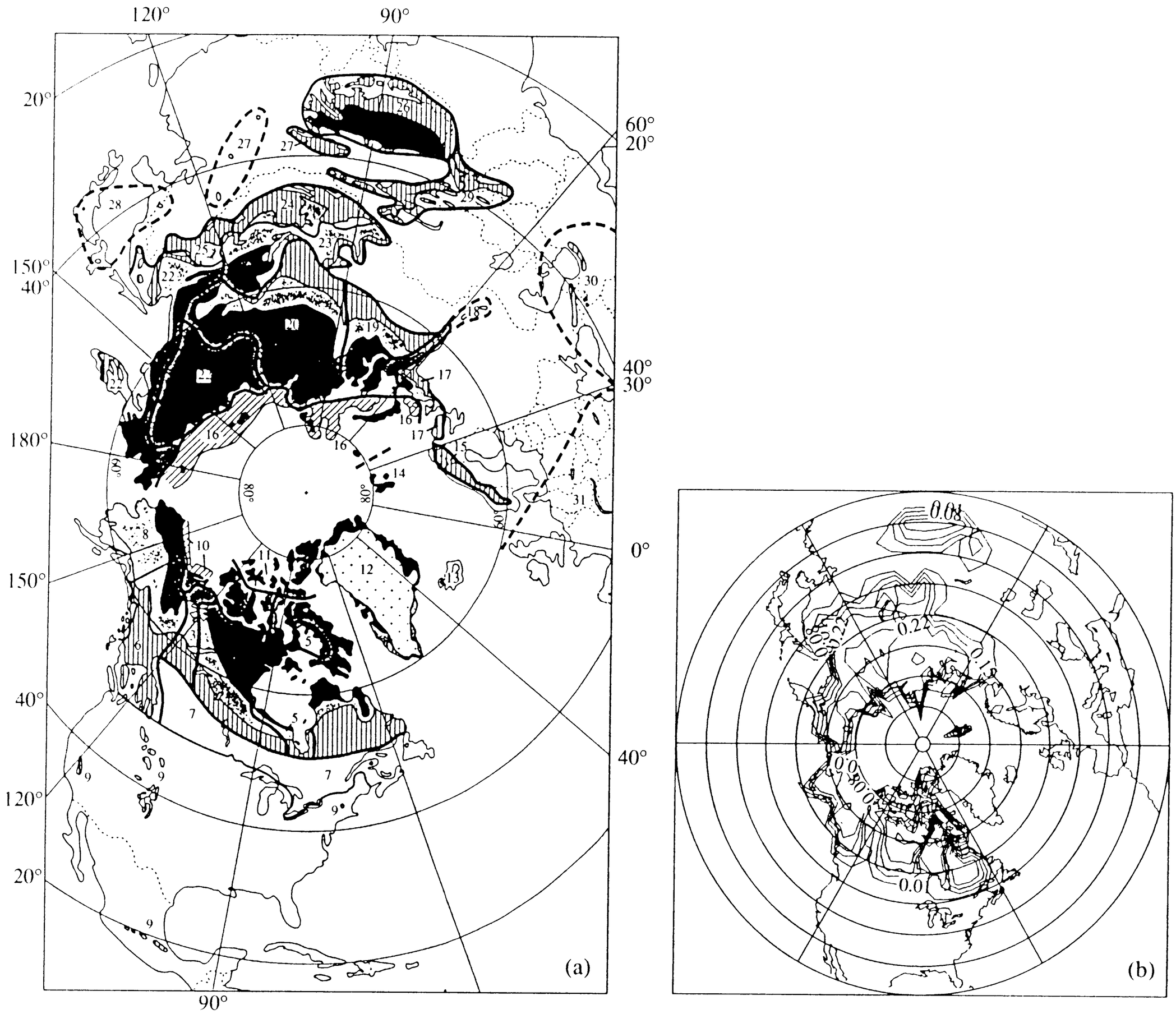

Fig. 5. (a) Observed permafrost distribution: individual permafrost areas (vertical shading), permafrost with gaps (gray), and continuous permafrost (black); (b) simulated ice distribution at a depth of 2 m for September.

large heat fluxes. An analysis of the heat flux distribution to the soil (not shown) revealed that its midlatitude magnitudes are 10–20 W/m^2.

It can also be seen in Fig. 2a that the differences between the simulated and observed surface air temperatures are small in the more southern regions. Moreover, a negative bias of 5–15 degrees over the Himalayas and China obtained in the control experiment as compared to the observed data was decreased or removed completely in experiment I. However, it should be noted that this bias over the Himalayas may be spurious and may result from the use of observational data obtained by a procedure that extrapolates from measurements conducted in valleys to the entire region, which leads to overestimated temperatures over high mountains.

The July differences between the simulated and observed temperatures (Fig. 2b) are considerably smaller than those obtained for the January circulation. Their values are no greater than two degrees in most of the regions. An exception is deserts and steppe regions, such as the southern United States, Arabia, and central Australia, where the calculated temperatures are 2–8 degrees greater than the observed ones. An analysis showed that the error of the reproduced surface air temperature over the southern United States in experiment I is caused by changes in convection, which manifest themselves in a decreased precipitation amount and a reduced soil-moisture evaporation rate as compared to those in the control experiment. For the other two regions, further investigations are required to clarify the causes of the bias and to reduce or remove it. Note that the July tem-

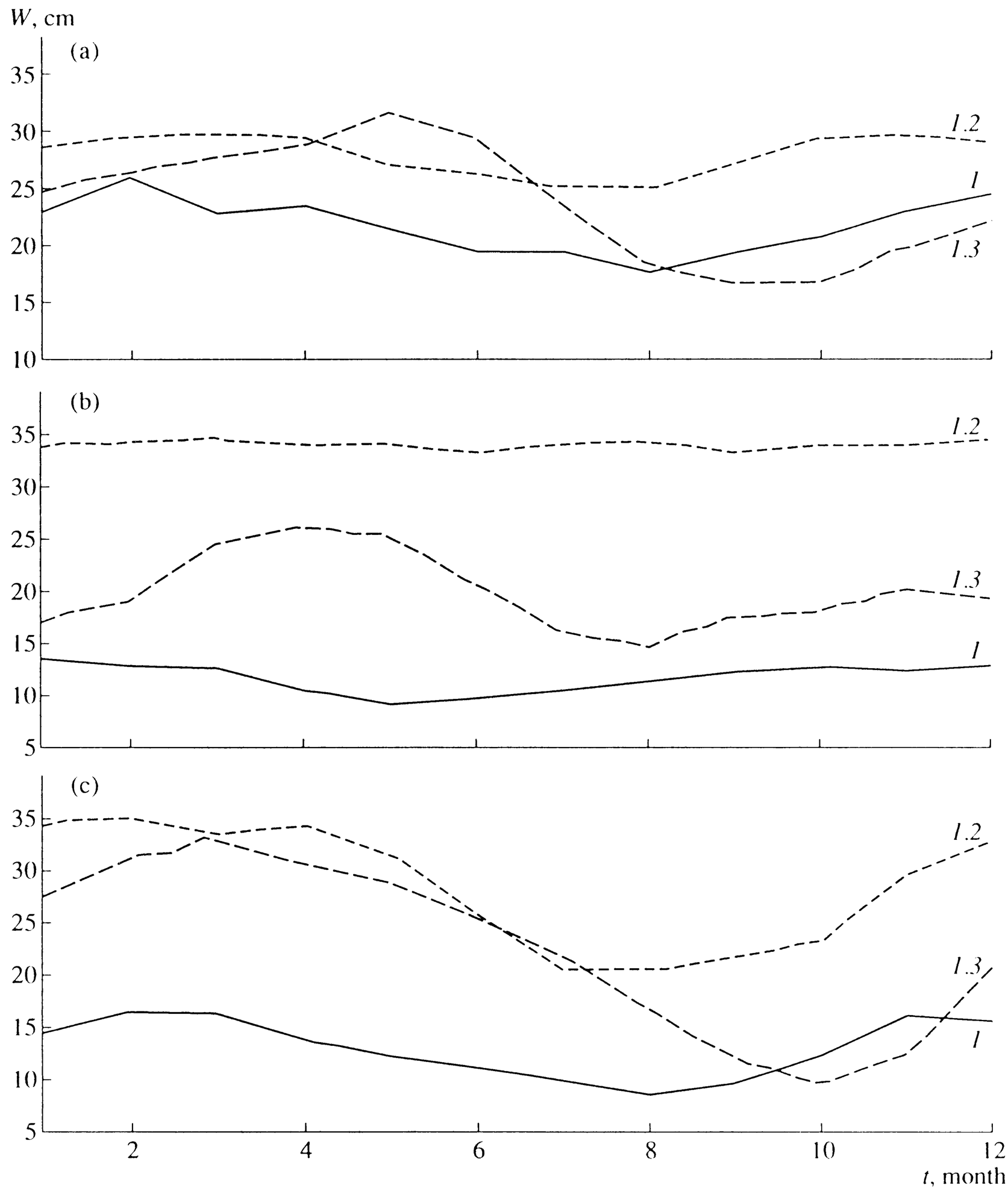

Fig. 6. Annual cycle of moisture within the upper one-meter soil layer for (a) northwest Russia (55°–65° N, 20°–60° E), (b) east China (32°–40° N, 105°–120° E), and (c) Illinois, USA (38°–40° N, 85°–90° W).

perature over the majority of vegetated areas in experiment I was 1–3 degrees larger than that in the control experiment. This is associated with the fact that the stomatal resistance in the control experiment was smaller, and, hence, the transpiration rate was higher.

An analysis showed that the mean July temperature simulated in experiment I is lower than that obtained in the control experiment for arid regions with a large fraction of inland waters. These regions are primarily those surrounding the Caspian Sea and those interpreted formally as land, because of the model horizontal resolution (5° longitude by 4° latitude), but actually including relatively small reservoirs such as the Aral Sea, Lake Chad, etc. As a rule, the simulated temperature is lower than the observed one for these regions, because the entire model grid square is characterized by a single temperature value, while the surface temperature of lakes is actually lower than that of the surrounding steppes and deserts. As a result, the model produces enhanced evaporation rates and reduced sensible heat fluxes in these regions, which leads to excess cooling of the surface.

As mentioned earlier, the temperature simulated for winter and summer in experiment I (detailed descrip-

Table 1. Percentages of sand, clay, and organic for eight soil types

No	Name	Sand	Clay	Organic
1	Coarse	83	9	8
2	Intermediate	37	30	33
3	Fine	17	67	16
4	Coarse–intermediate	60	20	20
5	Coarse–fine	50	38	12
6	Intermediate–fine	27	48	25
7	Coarse–intermediate–fine	46	35	19
8	Organic	16	16	68

tion of heat and moisture transfer in the soil) was generally higher than that obtained in the control experiment. This can be explained by more intense heat transfer from the soil for winter circulation and by reduced transpiration due to a larger stomatal resistance in summer. It is interesting that an increase in the heat flux to the soil in spring and summer is not as important as its decrease in winter, because the wintertime radiative balance is close to zero. Under these conditions, a 10–15 W/m^2 change in the heat flux from the soil is compensated by the corresponding changes in the surface temperature. In summer, when the radiative balance can reach 500 W/m^2 in the midday, the same changes in the heat flux from the soil can be easily compensated by small variations in the sensible and latent heat fluxes with virtually no influence on the surface temperature.

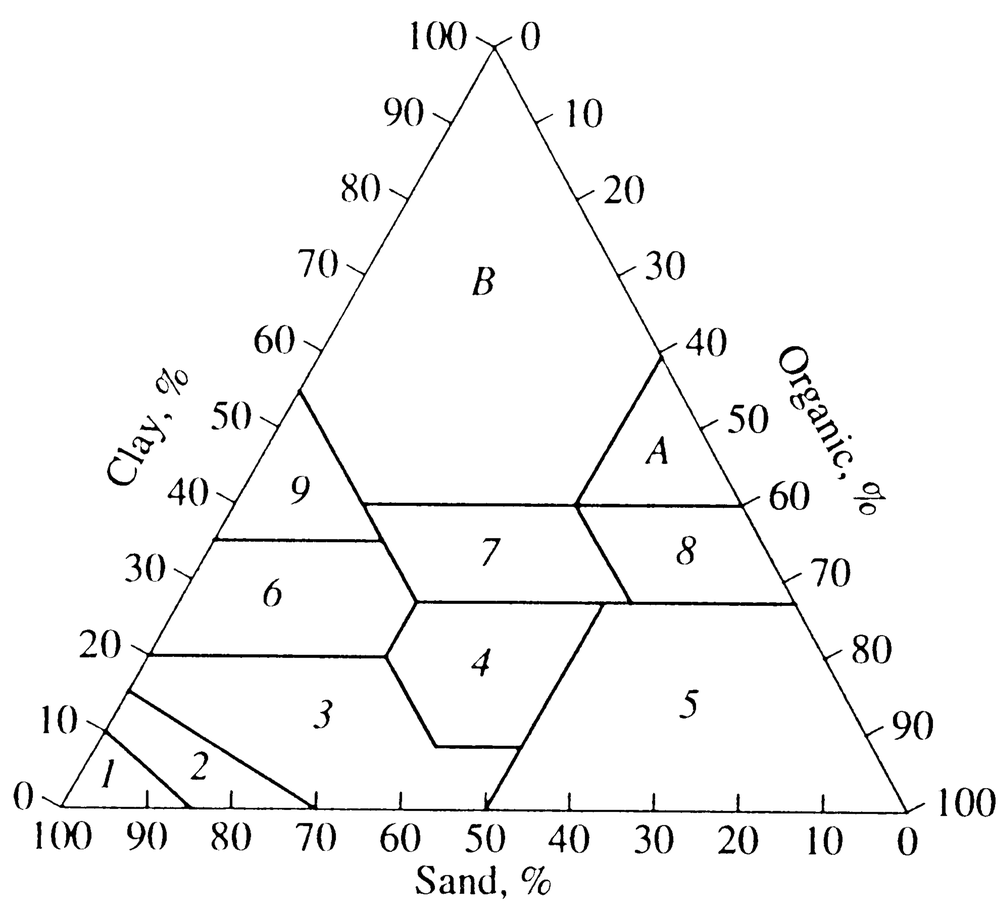

Fig. 7. Soil classification into 11 types depending on the percentages of sand, clay, and organic: (*1*) sand, (*2*) sand with loam, (*3*) loam with sand, (*4*) loam, (*5*) loam with humus, (*6*) loam with sand and clay, (*7*) loam with clay, (*8*) loam with clay and humus, (*9*) sand with clay, (*A*) humus with clay, and (*B*) clay.

2. SIMULATED HYDROLOGIC CYCLE OF THE LAND

Consider certain elements of the hydrologic cycle simulated in experiment I. Figures 3a and 3b compare zonally averaged precipitation fields calculated from model outputs and observational data for January and July, respectively. Figure 4 shows contour maps of differences between the simulated and observed monthly mean precipitation [5]. It is evident from the figures that the precipitation is well reproduced on the whole in the model. For example, the zonally averaged curves north of the equator for July (Fig. 3b) virtually coincide, and the simulated precipitation values are somewhat smaller as compared to the observations over the midlatitude oceans in the Northern Hemisphere for January (Fig. 3a). Taking into account that the July precipitation in the midlatitudes depends primarily on the soil moisture evaporation over the continents, we can consider the model to describe this process quite satisfactorily. In the Southern Hemisphere, there are sufficiently large systematic differences between the calculated and observed precipitation. We should note certain possibly spurious model errors associated with small redistributions of precipitation along the intertropical convergence zone. The simulated precipitation amounts in the tropics are on the whole smaller than the observed data. Note that the latter may not be reliable over the tropical oceans.

Figure 5 qualitatively compares the observed geographic permafrost distribution [6] (Fig. 5a) with that simulated in experiment I (Fig. 5b). The contours of soil ice content at a depth of 2 m for late September (Fig. 5b), when this quantity is minimum, show that the model reproduces well the geographic location of the permafrost boundary, at least over Russia.

Figure 6 presents the annual cycle of the moisture content within the upper one-meter soil layer simulated in experiment I and the control experiment, and the observed annual cycle for three regions in which regular measurements were conducted [7, 8]: (a) northwestern Russia (55°–65° N, 20°–60° E); (b) east China (32°–40° N, 105°–120° E); and (c) Illinois, USA (38°–40° N, 85°–90° W). For the control experiment, the soil moisture content is given for the entire two-meter soil layer with a water capacity of 0.35 m. The figure shows that the detailed soil–vegetation parametrization scheme correctly reproduces the amplitude and phase of the annual cycle of soil moisture over Russia and Illinois, but its magnitude has a positive bias. A possible cause of this qualitative discrepancy is that the observed moisture is meant as available moisture, i.e., the difference between the complete moisture content and its magnitude at the wilting point. The computed moisture content over eastern China is virtually constant and considerably exceeds the observed values, which is possibly associated with a positive bias in the simulated precipitation (Fig. 4).

Table 2. Soil type parameters

NN	b	$\psi_{max} \times 100$	Π	$\gamma_{max} \times 100$	$\lambda_{max} \times 10000$	W_0	W_m
1	4.05	3.50	0.395	0.01760	0.29800	0.02	0.01
2	4.38	1.78	0.410	0.01560	0.13900	0.05	0.02
3	4.90	7.18	0.435	0.00340	0.13700	0.08	0.03
4	5.39	14.6	0.451	0.00069	0.06190	0.20	0.08
5	5.30	56.6	0.485	0.00072	0.20400	0.18	0.07
6	7.12	8.63	0.420	0.00063	0.03070	0.13	0.06
7	8.52	36.1	0.476	0.00024	0.03720	0.27	0.12
8	7.75	14.6	0.477	0.00017	0.01240	0.24	0.11
9	10.4	6.16	0.426	0.00021	0.00641	0.23	0.10
A	10.4	17.4	0.492	0.00010	0.00755	0.30	0.15
B	11.4	18.6	0.482	0.00013	0.00926	0.40	0.20

Table 3. Model vegetation parameters

NN	a	b	c	C_{Fq}	ψ_b	ψ_w	Lt_{max}	z_r
1	2336	0.01	154	0.0273	–100	–500	4.5	1.0
2	9802	10.60	180	0.0357	–190	–250	4.0	1.0
3	6336	7.10	207	0.0340	–200	–250	5.0	1.0
4	2870	3.70	233	0.0310	–200	–250	7.0	1.0
5	2870	3.70	233	0.0310	–200	–250	2.0	0.5
6	56651	10.80	165	0.0357	–190	–250	3.0	3.0
7	2582	1.09	110	0.0238	–120	–230	3.0	0.5
8	93989	0.01	855	0.0275	–200	–400	0.8	2.0
9	93989	0.01	855	0.0275	–200	–400	1.0	2.0
10a	9802	10.55	180	0.0275	–200	–400	1.5	0.5
10b	2582	1.09	110	0.0238	–0.3	–150	0.4	0.5
11a	9802	10.60	180	0.0357	–190	–250	0.5	1.0
11b	7459	5.70	25	0.0000	–100	–200	3.0	1.0

3. MODEL SENSITIVITY

We carried out experiment II for three years to clarify the sensitivity of the model to the specification of various soil and vegetation types. The only difference between experiments I and II was that all soil parameters corresponded to loam (type 4, see Appendix 1) and the vegetation was specified by the same type—broadleaf deciduous forest. The vegetation cover fraction of the grid square was not varied. An analysis of contour maps of the differences between the surface air temperatures computed in experiments I and II (not shown) for all four seasons showed the following features. In the midlatitudes, this difference is mainly 1–4 degrees in winter and spring and no greater than 1–2 degrees in summer and fall. In the tropics, the differences are considerably smaller and do not exceed one degree almost everywhere virtually regardless of the season. Taking into account that the rms deviation of the simulated seasonally averaged temperature in the midlatitudes is about two degrees in winter and spring and about one degree in summer and fall and that this quantity in the tropics is about 0.5 degree, we can establish that, in many regions, these temperature variations are statistically significant despite their small values. Note that a temperature decrease by about one degree over Eurasia and North America in summer in the case when actual soil and vegetation are used can be explained by the fact that the stomatal resistance of the plants growing in these regions is somewhat smaller than that of broadleaf forests. The temperature variations in the tropics are also associated primarily with changed stomatal resistance. Further investigations are required to understand the causes of temperature variations in the midlatitudes in winter, fall, and spring. On the whole, the results of experiments I and II suggest that the averaged characteristics of the model atmosphere (for the horizontal and vertical resolutions used) are not very sensi-

tive to the degree of detail in the specification of soil and vegetation types.

In conclusion, we note that the described version of the soil–vegetation parametrization was designed so that it can be used in a stand-alone mode or within an atmospheric GCM. The ideas employed in designing this parametrization scheme allowed substantial improvement of the climate model being developed at the Institute of Numerical Mathematics, Russian Academy of Sciences. However, further efforts are required to improve the above computational algorithms for calculating heat and moisture transfer processes in the soil–vegetation system. As immediate prospects, we intend to incorporate a separate calculation of vegetation temperature that involves the radiative exchange of plants with air and soil, to assign different temperatures to different surface types within the grid square, and to change albedo calculations for the snow-covered surface and heat-transfer calculations through sea ice.

APPENDIX 1. SOIL TYPES USED IN THE MODEL

The soil classification is based on the data given in [9], which contain various soil characteristics down to a depth of 0.3 m on a one-degree grid. We used only the soil texture data, which include eight soil types, depending on the percentages of sand, clay, and organic. Their values are listed in Table 1. For soil textures containing large stones or representing sand dunes, the sand percentage was increased by 15%, of which 7% and 8% were taken from the clay and organic percentages, respectively. Thus, the percentages of clay, sand, and organic were considered known in each one-degree square. The soil composition at any model grid point was obtained by averaging the soil component over individual grid squares of the model.

However, it is well known that that the soil composition varies with depth. As a rule, the organic percentage decreases with depth and is close to zero below the upper fertile layer. For this reason, the component percentages obtained from [9] and characterizing the soil layer down to 0.3 m were assigned to a depth of 0.15 m in the model. It was also assumed that the organic percentage decreases linearly to zero at a certain depth, which was independent of the soil type and equals 0.7 m in this model version. The sand and clay percentages were taken the same at all soil levels.

Means of the model parameters that are necessary to calculate heat and moisture transfer in the soil were reported in [10, 11] for 11 soil types. Figure 7 illustrates the classification of these soils depending on the sand, clay, and organic fractions. The model soil at each grid point and each level was assigned to one of the 11 types, each of which is characterized by the parameters listed in Table 2. Here, b is Clapp–Hornberger's dimensionless constant, ψ_{max} is the maximum water potential (m), Π is the porosity in dimensionless units, γ_{max} is the maximum hydraulic conductivity (m/s), λ_{max} is the maximum diffusivity of water (m^2/s), W_0 is the amount of unfrozen water at zero temperature (kg/kg), and W_m is the amount of unfrozen water at very low temperatures (kg/kg).

APPENDIX 2. VEGETATION TYPES USED IN THE MODEL

The original data we used were an annual mean vegetation distribution given on a one-degree grid [2]. This distribution provides a dominant vegetation type (occupying more than half of the corresponding territory) and the vegetation type next in abundance (occupying from 25 to 50% of the territory), both specified at each grid point. Note that the latter quantity may occasionally coincide with the former. All the diversity of vegetation was classified into about 50 types. In addition, the following surface types could be specified: bare areas, inland water, perpetual ice, and large cities. Unfortunately, the vegetation data necessary for the model are available only for a coarser partition into 11 types (see [13]). In [12], a table was proposed that reduces 50 vegetation types to 24 coarser types. We used the principle for the construction of this table in order to assign each of the 24 types to one of the 11.

To obtain the fraction of each grid square covered by each vegetation type, the dominant vegetation type was considered to occupy the two-thirds of the one-degree square, and the vegetation type next in abundance, the remaining one-third of the square. After the 50 vegetation types had been reduced to 11, the result was averaged over all one-degree squares contained in a larger grid square of the model. In addition to vegetation, allowance was made for bare areas and inland waters.

Table 3 lists the model parameters dependent on the vegetation type and their values. Here, 1 signifies tropical rainforest; 2, broadleaf deciduous forest; 3, mixed broadleaf deciduous and needleleaf evergreen forest; 4, needleleaf evergreen forest; 5, needleleaf deciduous forest; 6, savanna trees; 7, grass; 8, broadleaf deciduous shrubs and grass; 9, broadleaf deciduous shrubs with bare areas; 10, tundra; and 11, crops with singly growing trees. Types 10 and 11 are subclassified into (a) trees or shrubs and (b) grass. The other designations have the following meanings: a (J/m^3), b (W/m^2), and c (s/m) are the parameters characterizing the dependence of the stomatal resistance on the incoming radiation; C_{Fq} (mb^{-1}) is the coefficient determining the dependence of the stomatal resistance on air humidity; ψ_b is the soil water potential at which the plants begin to wilt; ψ_w (m) is the soil water potential at the wilting points; Lt_{max} is the maximum leaf area index, which equals the leaves-to-soil-area ratio; and z_r (m) is the depth to which the plant roots extend.

ACKNOWLEDGMENTS

The initial distributions of vegetation and soil types over the land were obtained from an NCAR data set via

the Internet. We are grateful to Dennis Joseph for his timely sending of the description of soil-type data [9], as well as to the reviewer for the remarks made.

This work was supported by the Russian Foundation for Basic Research, project nos. 95-05-14172 and 96-05-64898.

REFERENCES

1. Volodin, E.M. and Lykosov, V.N., Parametrization of Heat and Moisture Transfer in the Soil–Vegetation System for Use in Atmospheric General Circulation Models: 1. Formulation and Simulations Based on Local Observational Data, *Izv. Akad. Nauk, Fiz. Atmos. Okeana*, 1998, vol. 34, no. 4, pp. 453–465 [*Izv., Atmos. Ocean. Phys.* (Engl. Transl.), vol. 34, no. 4, pp. 405–416].
2. Galin, V.Ya., Volodin, E.M., Lykosov, V.N., and Alekseev, V.V., *Razrabotka i sozdanie modeli obshchei tsirkulyatsii atmosfery A5413* (Development of the A5413 Atmospheric General Circulation Model), Available from VINITI, 1995, Moscow, no. 01.9.40 003086.
3. Jones, P.D., Raper, S.C.B., Bradley, R.S., Diaz, H.F., Kelly, P.M., and Wigley, T.M.L., Northern Hemisphere Surface Air Temperature Variations, 1851–1984, *J. Clim. Appl. Meteorol.*, 1986, vol. 25, pp. 161–179.
4. Jones, P.D., Raper, S.C.B., Bradley, R.S., Diaz, H.F., Kelly, P.M., and Wigley, T.M.L., Southern Hemisphere Surface Air Temperature Variations 1851–1984, *J. Clim. Appl. Meteorol.*, 1986, vol. 25, pp. 1213–1230.
5. Legates, D.R. and Willmott, C.J., Mean Seasonal and Spatial Variability in Gage-corrected, Global Precipitation, *Int. J. Climatol.*, 1990, vol. 10, no. 2, pp. 111–127.
6. Glaciological Data, *Workshop on Permafrost Data Rescue and Access, Report GD-28*, 1995, p. 3.
7. Hollinger, S.E. and Scott, A.I., A Soil Moisture Climatology of Illinois, *J. Clim.*, 1994, vol. 7, pp. 822–833.
8. Vinnikov, K.Ya. and Yeserkepova, I.B., Soil Moisture: Empirical Data and Model Results, *J. Clim.*, 1991, vol. 4, pp. 66–79.
9. Zobler, L., A World Soil File for Global Climate Modelling, *NASA Technical Memorandum 87802*, 1986.
10. Clapp, R.B. and Hornberger, M.G., Empirical Equations for Some Soil Hydraulic Properties, *Water Resour. Res.*, 1978, vol. 14, pp. 601–604.
11. Cosby, B.J., Hornberger, G.M., Clapp, R.B., and Ginn, T.R., A Statistical Exploration of the Relationships of Soil Moisture Characteristics to the Physical Properties of the Soil, *Water Resour. Res.*, 1984, vol. 20, no. 6, pp. 682–690.
12. Wilson, M.F. and Henderson-Sellers, A., A Global Archive of Land Cover and Soils Data for Use in General Circulation Climate Models, *J. Clim.*, 1985, vol. 5, pp. 119–143.
13. Dorman, J.L. and Sellers, P.J.A., Global Climatology of Albedo, Roughness Length and Stomatal Resistance for Atmospheric General Circulation Models as Represented by the Simple Biosphere Model (Sib), *J. Appl. Meteorol.*, 1989, vol. 28, pp. 833–855.

Translated by I.V. Ruzanova